


## Radio Sounding Measurements of the Solar Corona Using Giant Pulses of the Crab Pulsar in 2018

Munetoshi Tokumaru<sup>1</sup>  · Kaito Tawara<sup>1,2</sup> ·  
Kazuhiro Takefuji<sup>3</sup> · Mamoru Sekido<sup>4</sup> ·  
Toshio Terasawa<sup>5</sup>

© Springer ●●●

**Abstract** Observations of the Crab pulsar at 327 MHz were made at the Toyokawa Observatory of the Institute for Space-Earth Environmental Research, during the solar occultation in mid-June 2018 to investigate the coronal plasma density in the weak sunspot cycle, Cycle 24. The dispersion measures (DMs) were determined using giant pulses detected from observations of the Crab pulsar. The systematic increase in DM over the background level, observed during the period of the closest approach of the Crab pulsar’s line-of-sight to the Sun, was ascribed to the effect of the coronal plasma. The coronal density model which assumed spherical symmetry was determined by fitting it to the DM data, and it was compared with those determined in past solar cycles. The best fit model had large estimation errors, and indicated a systematically higher value than coronal densities derived from past observations. The results obtained here are likely to be significantly affected by latitude/longitude variation in coronal plasma density, the time variation of the interstellar medium, mainly the Crab nebula, and increased measurement errors due to the reduced occurrence of giant pulses. Hence, further observations are needed to derive conclusions about a change of coronal density in the current cycle.

**Keywords:** Solar Corona, Pulsar, Solar Wind

---

✉ M. Tokumaru  
tokumaru@isee.nagoya-u.ac.jp

<sup>1</sup> Institute for Space-Earth Environmental Research, Nagoya University, Nagoya, Japan

<sup>2</sup> Presently, TOBILA Systems

<sup>3</sup> Usuda Deep Space Center, Japan Aerospace Exploration Agency, Saku, Japan

<sup>4</sup> Kashima Space Technology Center, National Institute of Information and Communications Technology, Kashima, Ibaraki, Japan

<sup>5</sup> National Astronomical Observatory of Japan, Mitaka, Tokyo, Japan

## 1. Introduction

Solar activity during Cycle 24 (SC24) has been the lowest for the past 100 years, and some peculiar aspects of this cycle have been reported from in situ and remote sensing observations of the solar wind (e.g. McComas *et al.*, 2008, 2013; Tokumaru *et al.*, 2009, 2018; Tokumaru, Kojima and Fujiki, 2010, 2012; Tokumaru, Fujiki, and Iju, 2015; Janardhan *et al.*, 2011; Bisoi *et al.*, 2014). One of the marked peculiarities of SC24 is a significant drop in the solar wind density. Ulysses observations during the minimum between Cycles 23 and 24 (23/24), 2007–2008, demonstrated that the fast wind density from the polar coronal hole decreased by approximately 30 % when compared with the previous minimum (McComas *et al.*, 2008; 2013). Since a similar tendency was found from in situ observations in the ecliptic plane, the solar wind density was considered to have dropped globally during SC24. While Ulysses in situ measurements were no longer available after 2008, global observations of the solar wind have been conducted continuously using the interplanetary scintillation (IPS) method at the Institute for Space-Earth Environmental Research (ISEE) of Nagoya University. ISEE IPS observations revealed that the solar wind density fluctuation ( $\Delta N_e$ ) started declining from around 1995, and the trend continued in SC24 (Janardhan *et al.*, 2011; Bisoi *et al.*, 2014). Another analysis of ISEE IPS observations indicated that the occurrence of the very slow ( $<350$  km/s) solar wind associated with a low level of  $\Delta N_e$  significantly increased in SC 24, compared with SC23 (Tokumaru *et al.*, 2018). Since  $\Delta N_e$  is thought to be approximately proportional to the bulk density  $N_e$ , the results obtained from IPS observations are consistent with a global reduction in the solar wind density.

These facts suggest that a significant change may be taking place during SC24 at the solar corona, i.e. the source region of the solar wind, and hence an investigation of the coronal plasma density is needed to verify this. However, no in situ measurements within 0.3 AU are available yet except for the Parker Solar Probe (PSP). Even if PSP observations become available, it would be difficult to address the change in the global distribution of the coronal plasma density because its orbit is limited to within the ecliptic plane. Therefore, we have to rely on remote sensing observations of the solar corona. Although ISEE IPS observations cover a long period spanning more than three decades, the region within 0.2 AU is inaccessible to them due to the strong scattering effect. Observations of pulsars serve as an effective method for investigating the coronal plasma near the Sun (e.g. Counselman and Shapiro, 1968). The coronal density at 5–20 solar radii ( $R_S$ ) was determined from dispersion coefficient measurements for the Crab pulsar (PSR B0531+21) at Arecibo during the solar occultations in 1969, 1970, 1971, and 1973 (Counselman and Rankin, 1972, 1973; Weisberg, Payne, and Counselman, 1976). The coronal density near the Sun was also determined from time-of-arrival (TOA) measurements<sup>1</sup> for the millisecond pulsar

---

<sup>1</sup>Pulsar timing observations provide various kinds of information in astrophysics, Since a small change in integrated plasma density along the line-of-sight causes significant time delay in pulse arrival times, accurate correction of the solar wind variation is required for high precision pulsar timing (Madison *et al.*, 2019; Tuiburzi *et al.*, 2019).

PSR 1821-24 at Nançay in 1989, 1990, 1991, and 1992 (Cognard *et al.*, 1996). These observations were made at around the solar maximum in either SC20 or SC22. The coronal density profile at the solar minimum of SC23/24 was derived from TOA measurements for the Crab pulsar during the solar occultation in 2005 and 2007 at Pushchino (Smirnova, Chashei, and Shishov, 2009).

Observations of the Crab pulsar have been conducted since 2017 at the Toyokawa Observatory of ISEE to investigate the solar corona during SC24. This article presents the initial results obtained from the Crab pulsar observations at Toyokawa during the solar occultation in 2018. In this study, we derived dispersion measures (DMs) from the Crab pulsar observations at Toyokawa. The DM represents the line-of-sight (LOS) integrated electron density of the intervening plasmas between the pulsar and the observer:

$$\text{DM} = \int_0^L N_e ds, \quad (1)$$

where  $N_e$  is the electron density,  $s$  is the distance along the LOS, and  $L$  is the distance to the pulsar ( $L = 2$  kpc for the Crab pulsar; Lyne and Graham-Smith, 1998). The typical value of the DM for the Crab pulsar is  $56.79 \text{ pc cm}^{-3}$  (e.g. Isaacman and Rankin, 1977; McKee *et al.*, 2018). Note that the DM includes contributions from both interstellar and interplanetary plasmas. The amount of the interplanetary contribution depends on the solar elongation of the LOS, and becomes largest when the LOS is located closest to the Sun. For the Crab pulsar, observed DMs are mostly dominated by the interstellar contribution; the interplanetary contribution is only a minute fraction, i.e.  $\Delta\text{DM} \approx 10^{-2} \text{ pc cm}^{-3}$ , even at the closest approach to the Sun. In this study, we discriminated the interplanetary contribution from the interstellar one using data taken at large solar elongations, and we derived the plasma density profile of the solar corona in SC24.

The outline of this article is as follows. In Section 2, we describe the observation system employed for the present study. In Sections 3 and 4, we describe observations of the Crab pulsar at Toyokawa and the method for determining the DMs. In Section 5, we present DM data and the deduced coronal density profile. In Section 6, we compare the results obtained here with past observations of the Crab pulsar, and then compare them with IPS and coronagraph observations taken simultaneously. In Section 7, we summarize the results.

## 2. Instrumentation

In this study, we employed a radio telescope called the Solar Wind Imaging Facility Telescope (SWIFT, Tokumaru *et al.*, 2011) at the Toyokawa Observatory. SWIFT is designed for IPS observations and is used as one of the antennas that compose the multi-station system of ISEE (Tokumaru, 2013). The observation frequency of SWIFT is 327 MHz. SWIFT is composed of a cylindrical parabolic reflector with dimensions of 106 m (north-south)  $\times$  38 m (east-west) and a 192-element phased array receiver. The large effective area (1980 m<sup>2</sup>) of SWIFT

enables high-sensitivity detection of radio waves from the sources. A single beam formed by the phased array receiver is steerable only in the north-south direction, being fixed in the meridian plane. Therefore, observations with SWIFT for a given radio source are made once in a day within the time interval corresponding to its passage across the antenna beam. The observation time for the Crab pulsar is set to six minutes centered at its culmination. The 327 MHz signal from the phased array receiver is fed to a superheterodyne receiver, which converts it to a lower intermediate frequency (IF), 70 MHz. The IF signal with a bandwidth of  $\approx 20$  MHz is sampled by the high-speed sampler, ADS3000+ (Cosmo Research Inc.). In this study, we set the sampling rate and the bit depth to 256 Msps and 8 bit, respectively. The sampled data are recorded with the 10-TB RAID which is connected to the sampler via a 10 GB Ethernet.

### 3. Observations

Table 1 and 2 summarize the characteristics of the Crab pulsar and the parameters of the Toyokawa observations, respectively. The LOS for the Crab pulsar approaches the Sun on 15–16 June of every year, as close as  $\approx 5 R_{\odot}$ . Observations of the Crab pulsar at Toyokawa were made on a daily basis between 13 and 19 June 2018; MJD (modified Julian date) 58282–58288. Figure 1 shows the locations of the Crab pulsar’s LOS in the Sun-centered sky plane and the solar offset distance for the days when Toyokawa observations were made. In addition, Crab pulsar observations at Toyokawa were made for the period when the LOS was located far from the Sun, i.e. between 19 September 2017 and 15 July 2018 (MJD 58015–58314). The purpose of the Crab pulsar observations at large elongations is twofold: to remove the contribution of the interstellar medium from observed DMs and to evaluate the accuracy of the Toyokawa DM data. Crab pulsar observations made on 1 June and 1 July 2018 (MJD 58270 and 58300) were used to determine the level of the interstellar contribution during the solar occultation. Crab pulsar observations were made daily between 20 September and 12 March 2018 (except for 7–18 December 2018) and once a month after that, i.e. near the 15th day of every month. These observations were used for comparison with Jodrell Bank observations (Lyne, Pritchard, and Smith, 1993, <http://www.jb.man.ac.uk/~pulsar/crab.html>). The sparse density of the observations between March and July was caused by the meridian transit of the Crab pulsar occurring during daytime, when IPS observations were conducted as a priority for many sources. The total number of days for Crab pulsar observations was 170.

## 4. Analysis

### 4.1. Detection of Giant Pulses

The Crab pulsar is known as an active emitter of giant pulses (GPs), which are sporadic flashes of radio emission with a flux greatly exceeding the mean level

(e.g. Lundgren *et al.*, 1995; Cordes *et al.*, 2004). Such a high signal to noise (S/N) ratio of GPs enables the quick and accurate determination of DMs from the observed data. We first retrieved the intrinsic time variation of the signal intensity of the Crab pulsar from the Toyokawa data by making a coherent correction of the frequency dispersion, i.e. a “dedispersion”. Here, we assumed  $DM = 56.79 \text{ pc cm}^{-3}$ . We identified pulses with  $S/N > 5$  from the retrieved data. The identified pulses whose pulsar phases are located neither at  $180 \pm 18^\circ$  (main pulse) nor  $324 \pm 18^\circ$  (inter-pulse) were regarded as false detections due to radio frequency interference, and hence they were rejected. The remaining pulses were regarded as GPs. Figure 2 shows an example of a GP identified from Crab pulsar observations at Toyokawa (on 20 September 2018). In total, 47123 GPs were detected from the Crab pulsar observations at Toyokawa.

## 4.2. Determination of DMs

Among the detected GPs, we determined DMs for the selected GPs with  $S/N > 15$  by searching for an optimal value which maximizes the peak height of the pulse. The use of data with such an excellent S/N enables reliable determination of DMs. When searching for the optimal value, we made the coherent dedispersion repeatedly changing a DM from 56.6 to 57.0  $\text{pc cm}^{-3}$  in steps of 0.002  $\text{pc cm}^{-3}$ . The DM determination was made for seven days around the closest approach to the Sun in June 2018 and also on days near those of the Jodrell Bank observations, i.e. the 15th day of every month. We calculated the daily means and standard errors of the optimal values and used them as the DM data in this study. Table 3 shows the DM data, which include the daily means and standard errors. The DM data for 13 June 2018 was discarded since the number of GPs with  $S/N > 15$  was too small ( $N=3$ ).

## 5. Results

### 5.1. Occurrence Rate of GPs

We calculated the occurrence rate of GPs with  $S/N > 5$  by dividing the number of GPs by the observation time (360 s) on a daily basis. Figure 3 shows the time variation of the occurrence rate of GPs. The occurrence rates exhibited variability on various time scales, and they decreased significantly during the solar occultation period. The highest rate, 1.29/s, occurred at MJD 58130 (12 January 2018), and the lowest rate, 0.15/s, at MJD 58284 (15 June 2018). The average rate of 0.77/s over the analysis period means that one GP with  $S/N > 5$  occurs among  $\approx 40$  pulses. The ratio of main pulse (MP) to inter-pulse (IP) GPs is approximately 7:3. The variability of GP occurrence rates may be ascribed to the scattering effect in the interstellar medium, predominantly in the Crab nebula (Isaacman and Rankin, 1977; Kuz'min *et al.*, 2011; McKee *et al.*, 2018), however further discussion on this fact is beyond the scope of this article.

Figure 4 shows the S/N distribution for MP and IP GPs. Power-law distributions are clearly revealed from the figure for both MP and IP GPs. The

distribution for MP GPs exhibited a clear break at  $S/N = 10$ , and the index varied from  $-2.0$  at  $S/N < 10$  to  $-2.9$  at  $S/N > 10$ . The distribution for IP GPs did not show any change in the index, and it was well explained by a single power law with an index of  $-3.2$ . A similar change in the index for MP GPs was reported from Crab pulsar observations at 600 MHz (Popov *et al.*, 2009). However, the indices derived here are different and systematically steeper than those obtained in the earlier study:  $-1.3$  and  $-2.4$  at low and high energies, respectively, for MP and  $-2.4$  for IP. This may be ascribed to the difference in the observation frequency.

## 5.2. DMs and the Coronal Density Profile

In Figure 5, the DMs derived from the Crab pulsar observations at Toyokawa are plotted as a function of time for the period between September 2017 and July 2018. As shown here, Toyokawa DMs gradually declined until March 2018 (MJD  $\approx 58200$ ) and rose after that. The day of the closest approach to the Sun is indicated by the vertical dotted line. The observed DMs increased at around the period of the closest approach, and this DM increase is ascribed to the effect of the coronal plasma, while the data are associated with a large standard error. The larger errors during the solar occultation are mostly ascribed to the decrease in GP occurrence (see Section 5.1). The Jodrell Bank data indicated in the figure are in good agreement with the Toyokawa data and show a similar trend, i.e. a gradual decline and rise is also revealed from the Jodrell Bank data. The error of Jodrell Bank data is typically  $0.005 \text{ pc cm}^{-3}$  (Lyne, Roberts, Jordan, 2018), and this is comparable to the errors of Toyokawa DM data (see Table 3). When the Toyokawa data with  $N > 20$  are selected, the difference between the Toyokawa and Jodrell Bank data taken over seven days is less than  $0.004 \text{ pc cm}^{-3}$ , and the mean difference is  $0.0007 \pm 0.002 \text{ pc cm}^{-3}$ . This suggests that Crab pulsar observations at Toyokawa provide reliable DM estimates when sufficient GPs with an excellent  $S/N$  are available. We note that there is a distinct difference in the time span for DM determination between Jodrell Bank and Toyokawa; the former is several days, whereas the latter is only one day. Hence, the two sets of DM data do not necessarily agree with each other if the DMs have a variability within a time scale of a few days.

We derived the DM excess  $\Delta\text{DM}$  during the solar occultation by subtracting the background level due to the interstellar contribution from the Toyokawa DM data. The background level was determined by linear interpolation using two DMs taken on 1 June and 1 July (MJD 58270 and 58300). Such a simple method to determine the background level may cause some uncertainties, since DMs of the Crab pulsar exhibit high variability (Isaacman and Rankin, 1977; McKee *et al.*, 2018). Figure 6 shows  $\Delta\text{DM}$  for 30 days approximately centered at the day of the closest approach to the Sun (vertical dotted line). We fit the following density model to the  $\Delta\text{DM}$  data,

$$N_e(r) = N_0 \left( \frac{r}{r_0} \right)^{-\alpha}, \quad (2)$$

where  $N_0$  is the electron density at  $r_0 = 10R_S$ , while  $\alpha$  and  $r$  are the power-law index and the radial distance, respectively. This model assumes spherical symmetry of the coronal plasma distribution, and it has been used in many earlier studies (e.g. Counselman and Rankin, 1972, 1973; Cognard *et al.*, 1996; Smirnova, Chashei, and Shishov, 2009). An advanced density model taking the two states of the solar wind into account was used to analyze pulsar DM data (Tiburzi *et al.*, 2019). However, the two-state model did not perform better than the spherically symmetric model in their study. Therefore, we consider that the spherically symmetric model given in Equation 2 is a safe choice. In this study,  $N_0$  and  $\alpha$  are assumed to be free parameters.

The best fit model is plotted by the solid curved line in the figure. The best-fit parameters are  $N_0 = (7.8 \pm 7.9) \times 10^3 \text{ cm}^{-3}$  and  $\alpha = 1.7 \pm 1.3$ . It can be clearly seen from the figure that this model poorly fits the observed  $\Delta\text{DM}$  data, and hence the estimation errors for these parameters are quite large. One reason for this could be that this model assumes a spherically symmetric distribution of the coronal plasma density. It is well known that, particularly at the solar minimum, the structure of the solar corona deviates from spherical symmetry. Deviation of observed DM variations from the spherically symmetric model was examined from pulsar timing observations (Madison *et al.*, 2019; Tiburzi *et al.*, 2019). We will address the effect of longitude and latitude structure of the solar corona in the next section. Another reason for the estimated errors is the effect of short-term variations in the interstellar plasma. Rapid and large DM variations of the Crab pulsar, compared to those of other pulsars, were found, and these were ascribed to discrete structures within the Crab nebula (Isaacman and Rankin, 1977; McKee *et al.*, 2018). The other reasons are reduced reliability caused by a decrease in the occurrence of GPs during the solar occultation period and a limited number of Crab pulsar observations. Nevertheless, this model fit is useful for comparing our results with past observations, which are presented in the next section.

## 6. Discussion

### 6.1. Comparison with Past Observations

Figure 7 shows integrated coronal plasma densities derived from Crab pulsar observations made at Arecibo between 1969 and 1973, SC20 maximum (Counselman and Rankin, 1972, 1973; Weisberg, Payne, and Counselman, 1976), where the density data are plotted as a function of the day of the year (DOY). The integrated coronal densities show a peak on DOY 166 (the day of the closest approach to the Sun), and its level corresponds to  $\approx 10^{-2} \text{ pc cm}^{-3}$ . The best fit model of the coronal density determined in this study is indicated by the solid curved line in the figure. The result of this study is close to the density data from the past observations, but it appears to provide a systematically larger density for the coronal plasma than those. Since the best fit model contains large uncertainties, we cannot safely attribute this difference to an intrinsic change in the solar corona. Crab pulsar observations at Jodrell Bank reported an increase

in DM of  $0.045 \text{ pc cm}^{-3}$  within  $5^\circ$  of the Sun (Lyne, Pritchard and Smith, 1988), which is generally consistent with our DM data. The observed  $\Delta\text{DMs}$  are larger than the solar wind DM estimated by the pulsar software Tempo2 (Edwards, Hobbs, and Manchester, 2006). In Tempo2, the solar wind density is assumed to vary as  $r^{-2}$  and higher-order terms such as  $r^{-4}$  and  $r^{-6}$  (Leblanc, Dulk, and Bougeret, 1998) are not included. The higher order terms represent effects of the super-radial expansion of flux tube and the solar wind acceleration, and they becomes prominent at small distances. The discrepancy between observed  $\Delta\text{DMs}$  and Tempo2 estimates is ascribed to the contribution of the higher-order terms.

Table 4 summarizes parameters  $N_0$  and  $\alpha$  of the coronal density model determined by pulsar observations including those in this study. As shown here,  $N_0$  and  $\alpha$  obtained from earlier studies tend to be low and flat at solar minimum or in the declining phase, and high and steep at solar maximum. This tendency is ascribed to the effect of the rarefied region associated with coronal holes which develop over the poles during the low solar activity period. The value of -1.7 determined for  $\alpha$  in this study is relatively flat, compared with those observed at solar maxima, and this is consistent with the effect of polar coronal holes. The value of  $N_0$  in this study is as high as those at the solar maxima, which is inconsistent with the solar cycle variation of  $N_0$  revealed from earlier studies and also inconsistent with what is expected from the marked drop of the solar wind density in SC24. We consider that this discrepancy may arise from the uncertainty of the model fit, as mentioned above, and hence we need to make further observations to investigate the long-term change in the solar corona.

## 6.2. Comparison with IPS and Coronagraph Observations

To examine the effect of the latitude and longitude variation in the coronal plasma on Crab pulsar observations, we analyzed two kinds of data: the solar wind speed data obtained from IPS observations and the whitelight intensity data from coronagraph observations. Figure 8 shows the Carrington source surface map of the solar wind speeds derived from ISEE IPS observations (Kojima and Kakinuma, 1990; Tokumaru, 2013) for Carrington rotation (CR) 2204. To produce this map, we employed computer-assisted tomography (CAT) analysis, which enables correction of the LOS integration effect inherent to the IPS observations (Kojima *et al.*, 2007). The source surface is assumed to be at  $2.5 R_S$  in the CAT analysis. Color represents the solar wind speed, and the white area corresponds to the region where no data are available. We note that the period of the Crab pulsar’s solar occultation in 2018 corresponds to CR 2205. The solar wind speed data for CR 2205 were available, but the latitude and longitude coverage of IPS observations for CR 2205 was poor. In this study, we employed the solar wind speed data of CR 2204 for comparison with the Crab pulsar observations, since the data for CR 2204 had a better latitude and longitude coverage than those for CR 2205. The solar wind structure at solar minimum is known to be stable, and the overall feature of the solar wind speed distribution revealed from CR 2205 data was quite similar to that for CR 2204. Hence, the difference in the solar wind speed distribution between CR 2204



and 2205 is considered to be sufficiently small. The projected locations of LOS for the Crab pulsar at the time of the Toyokawa observations between 13 and 19 June 2018 are indicated by dotted lines in the figure, and a solid circle on each LOS represents the projected location of the closest approach to the Sun, which is known as the P-point. The density variation along the LOS indicates a maximum at the P-point, and this peak becomes sharp for the LOS with a small solar elongation, as illustrated in Figure 9. Therefore, the DM data taken for the region near the Sun are considered to be dominated by the contribution at the P-point. In projecting the LOS locations onto the source surface, the longitudinal shift caused by the solar rotation was not taken into account. The effect of the solar rotation causes a significant change in the projected location of the source surface for large distances. However, it is negligible for the near-Sun region where the P-points of the Crab pulsar’s LOS are located. Unfortunately, the coverage of IPS observations even for CR 2204 is imperfect, particularly for the southern hemisphere, and the solar wind data are unavailable for most of the LOSs for the Crab pulsar observations on 13, 14, and 15 June. For the remaining days, the solar wind data are available for the entire LOS. As shown in the figure, LOSs for the Crab pulsar move from the fast-wind region to the slow-wind region during 16–19 June.

Figure 10 shows the Carrington maps of the Thomson-scattered whitelight intensity for CR 2205 measured by the Large Angle and Spectrometric Coronagraph (LASCO: Brueckner *et al.*, 1995). The whitelight intensity represents the integrated electron density of the solar corona along the LOS. Here, we used data from the C3 imager at  $5 R_S$  on the west limb. The reason for the use of the west limb data is that its reference date was closer to the period of Crab pulsar observations than that of the east limb data. There was no significant difference when we used the east limb data. The height of  $5 R_S$  corresponds to the minimum distance of the P-point for the Crab pulsar, and the coronal features revealed at  $5 R_S$  were almost the same as those at different heights within  $10 R_S$ . The coverage of this map is better than the solar wind speed map (Figure 8), although this map includes the LOS integration effect. The P-points of the Crab pulsar’s LOS between 13 and 19 June are indicated on this map. As shown here, the LOSs for the Crab pulsar around the P-point were mostly immersed in the dark region until 16 June, and those for 18 and 19 June passed through the bright region, i.e. the helmet streamer near the equator. Thus, the Crab pulsar observations in June 2018 are likely to be significantly influenced by the longitude and latitude variation of the coronal plasma.

Figure 11 shows time variation of the whitelight intensities at  $5 R_S$  and the solar wind speeds on the source surface for the P-points of the Crab pulsar’s LOS during 13–19 June 2018. The whitelight intensities rapidly increased after MJD 58284 (15 June 2018), showing a maximum at MJD 58288 (19 June 2018), and this suggests that the LOS for the Crab pulsar entered the high-density region associated with the equatorial streamer. In contrast, the solar wind speeds dropped suddenly on MJD 58288, suggesting a close association between the helmet streamer and the slow solar wind (Sime and Rickett, 1981; Eselevich, Eselevich and Fujiki, 2007). The Toyokawa DM data on MJD 58288 displayed distinct deviation from the model value toward a higher density (see Figure 6),

and this deviation may be ascribed to the effect of the dense plasma associated with the helmet streamer. If this data is discarded, the model fit yields a smaller density and a steeper slope,  $N_0 = 7.1 \pm 5.4 \times 10^3 \text{ cm}^{-3}$  and  $\alpha = 3.3 \pm 2.2$ .

## 7. Summary

We performed observations of the Crab pulsar at 327 MHz using SWIFT at Toyokawa for the period between September 2017 and July 2018, which included the closest approach of the LOS to the Sun. The primary purpose of these observations was to investigate the distribution of the coronal plasma density near the Sun during SC24, when the solar activity declined remarkably. Many GPs were detected from the Crab pulsar observations, and their occurrence rates significantly varied in time from 1.29/s to 0.15/s. This variability is mainly ascribed to the effect of the Crab nebula. The power-law distributions of the S/N were determined for both MP and IP GPs. The indices for MP and IP GPs were systematically steeper than those reported from earlier studies, which may be due to the dependence of the observation frequency. The power-law index of MP GPs for  $S/N < 10$  was flatter than that for  $S/N > 10$ , and this was consistent with earlier observations. We determined DMs from the Crab pulsar observations for 18 selected days by optimizing the peak level of GPs with  $S/N > 15$ . The derived DMs around the period of the closest approach increased above the background level, and this increase is ascribed to the effect of the coronal plasma. We determined the radial profile of the coronal plasma density by fitting the spherically symmetric model to the excess DM data, and then we compared this with past observations. The model gave a systematically higher value of the coronal density than past observations, and this is a clear difference from the solar wind observations which showed a distinct drop in density in SC24. Furthermore, the model was associated with large uncertainties. The result obtained here is likely to be significantly influenced by various factors such as latitude and longitude variation of the coronal plasma density, time variation of the interstellar medium, i.e. the Crab nebula, and increased measurement errors caused by a reduction in GP occurrence. Therefore, further observations are needed to draw reliable conclusions about the coronal plasma density of SC24.

**Acknowledgments** This work was partly supported by a Grant-in-Aid for Scientific Research (A) (25237079) and also partly by the ISEE director's leadership fund for FY2015. The DM data for the Crab pulsar at Jodrell Bank Observatory were obtained from <http://www.jb.man.ac.uk/~pulsar/crab.html>. The IPS observations were conducted under the solar wind program of the ISEE. Solar wind data derived from ISEE IPS observations were available from <ftp://ftp.isee.nagoya-u.ac.jp/pub/vlist>. The WSO observations were obtained from <http://wso.stanford.edu/synsourcel.html>. The synoptic map of LASCO C3 observations was obtained from <https://lasco-www.nrl.mil>. The authors would like to thank Ms. Yuka Miyauchi (KSTC, NICT) and Mr. Yasushi Maruyama (ISEE, Nagoya Univ.) for their assistances.

**Disclosure of Potential Conflicts of Interest** The authors declare that they have no conflicts of interest.

## References

- Bisoi, S.K., Janardhan, P., Ingale, M., Subramanian, P., Ananthakrishnan, S., Tokumaru, M., Fujiki, K.: 2014, A study of density modulation index in the inner heliospheric solar wind during solar cycle 23, *Astrophys. J.*, **795**, 69 (doi:10.1088/0004-637X/795/1/69).
- Brueckner, G.E., Howard, R.A., Koomen, M.J., Korendyke, C.M., Michels, D.J., Moses, J.D., Socker, D.G., Dere, K.P., Lamy, P.L., Llebaria, A., Bout, M.V., Schwenn, R., Simnett, G.M., Bedford, D.K., Eyles, C.J.: 1995, The Large Angle Spectroscopic Coronagraph (LASCO), *Sol. Phys.*, **162**, 357 (doi:10.1007/BF00733434).
- Cognard, I., Bourgois, G., Lestrade, J.F., Biraud, F., Aubry, D., Darchy, B., Drouhin, J.P.: 1996, High-precision timing observations of the millisecond pulsar PSR 1821-24 at Nancay, *Astron. and Astrophys.*, **311**, 179.
- Cordes, J.M., Bhat, N.D.R., Hankins, T.H., McLaughlin, M.A., Kern, J.: 2004, The brightest pulses in the universe: multifrequency observations of the Crab pulsar's giant pulses, *Astrophys. J.*, **612**, 375 (doi:10.1086/422495).
- Counselman, C.C., Shapiro, I.I.: 1968, Scientific uses of pulsars, *Science*, **166**, 352 (doi:10.1126/science.162.3851.352-a).
- Counselman, C.C., Rankin, J.M.: 1972, Density of the solar corona from occultations of NP 0532, *Astrophys. J.*, **175**, 843 (doi:10.1086/151604).
- Counselman, C.C., Rankin, J. M.: 1973, Changes in the distribution of density and radio scattering in the solar corona in 1971, *Astrophys. J.*, **185**, 357 (doi:10.1086/152423).
- Edwards, R.T., Hobbs, G.B., Manchester, R.N.: 2006, TEMPO2, a new pulsar timing package II. The timing model and precision estimates, *Mon. Not. Roy. Astron. Soc.*, **372**, 1549 (doi:10.1111/j.1365-2966.2006.10870.x).
- Eselevich, M., Eselevich, V., Fujiki, K.: 2007, Streamer belt and chains as the main sources of quasi-stationary slow solar wind, *Solar Phys.*, **240**, 135 (doi:10.1007/s11207-006-0197-z).
- Isaacman, R., Rankin, J.M.: 1977, The Crab nebula pulsar: variability of dispersion and scattering, *Astrophys. J.*, **214**, 214 (doi:10.1086/155245).
- Janardhan, P., Bisoi, S. K., Ananthakrishnan, S., Tokumaru, M., Fujiki, K.: 2011, The prelude to the deep minimum between solar cycles 23 and 24: Interplanetary scintillation signatures in the inner heliosphere, *Geophys. Res. Lett.*, **38**, L20108 (doi:10.1029/2011GL049227).
- Kojima, M., Kakinuma, T.: 1990, Solar cycle dependence of global distribution of the solar wind speed, *Space Sci. Rev.*, **53**, 173 (doi:10.1007/BF00212754).
- Kojima, M., Tokumaru, M., Fujiki, K., Hayashi, K., Jackson, B.V.: 2007, IPS tomographic observations of 3D solar wind structure, *Astron. Astrophys. Trans.*, **26**, 467 (doi:1080/105567990701596200).
- Kuz'min, A. D., Belyatsky, Y.A., Dumsky, D.V., Izvekova, V.A., Lapaev, K.A., Logvinenko, S.V., Losovsky, B.Y., Pugachev, V.D.: 2011, Monitoring of the radio emission of the Crab nebula pulsar at low frequencies, *Astron. Rep.*, **55**, 416 (doi:10.1134/S1063772911040032).
- Leblanc, Y., Dulk, G.A., Jean-Louis Bougeret, J.: 1998, Tracing the electron density from the corona to 1 AU, *Solar Phys.*, **183**, 165 (doi:10.1023/A:1005049730506).
- Lundgren, S.C., Cordes, J.M., Ulmer, M., Matz, S.M., Lomatch, S., Foster, R.S., Hankins, T.: 1995, Giant pulses from the Crab pulsar: A joint radio and gamma-ray study, *Astrophys. J.*, **453**, 433 (doi:10.1086/176404).
- Lyne, A.G., Pritchard, R.S., Smith, F.G.: 1988, Crab pulsar timing 1982-87, *Mon. Not. Roy. Astron. Soc.*, **233**, 667.
- Lyne, A.G., Pritchard, R.S., Smith, F. G.: 1993, 23 years of crab pulsar rotational history, *Mon. Not. Roy. Astron. Soc.*, **265**, 1003 (doi:10.1093/mnras/265.4.1003).
- Lyne, A.G., Graham-Smith, F.: 1998, Pulsar astronomy, Cambridge University Press.
- Lyne, A.G., Roberts, M.E., Jordan, C.A.: 2018, Jodrell Bank Crab pulsar timing results, monthly ephemeris (<http://www.jb.man.ac.uk/pulsar/crab/crabnotes.ps>).
- Madison, D.R., Cordes, J.M., Arzoumanian, Z., Chatterjee, S., Crowter, K., DeCesar, M.E., Demorest, P.B., Dolch, T., Ellis, J.A., Ferdman, R.D., Ferrara, E.C., Fonseca, E., Gentile, P.A., Jones, G., Jones, M.L., Lam, M.T., Levin, L., Lorimer, D.R., Lynch, R.S., M. A. McLaughlin, M.A., Mingarelli, C.M.F., Ng, C., Nice, D.J., Pennucci, T.T., Ransom, S.M., Ray, P.S., Spiewak, R., Stairs, I.H., Stoval, K., Swiggum, J.K., Zhu, W.W.: 2019, The NANOGrav 11 yr data set: solar wind sounding through pulsar timing, *Astrophys. J.*, **872**, 150 (doi:10.3847/1538-4357/ab01fd).

- McKee, J.W., Lyne, A.G., Stappers, B.W., Bassa, C.G., Jordan, C.A.: 2018, Temporal variations in scattering and dispersion measure in the Crab pulsar and their effect on timing precision, *Mon. Not. Roy. Astron. Soc.*, **479**, 4216 (doi:10.1093/mnras/sty1727).
- McComas, D.J., Ebert, R.W., H. A. Elliott, H.A., Goldstein, B.E., Gosling, J.T., Schwadron, N.A., Skoug, R.M.: 2008, Weaker solar wind from the polar coronal holes and the whole Sun, *Geophys. Res. Lett.*, **35**, L18103 (doi:10.1029/2008GL034896).
- McComas, D. J., Angold, N., Elliott, H.A., Livadiotis, G., Schwadron, N.A., Skoug, R.M., Smith, C.W.: 2013, Weakest solar wind of the space and the current “mini” solar maximum, *Astrophys. J.*, **779**, 10 (doi:10.1088/0004-637X/779/1/2).
- Popov, M., Soglasnov, V., Kondratiev, V., Bilous, A., Moshkina, O., Oreshiko, V., Ilyasov, Y., Sekido, M., Kondo, T.: 2009, Multifrequency study of giant radio pulses from the Crab pulsar with the K5 VLBI recording terminal, *Pub. Astron. Soc. Japan*, **61**, 1197 (doi:10.1093/pasj/61.6.1197).
- Sime, D.G., Rickett, B.J.: 1981, Coronal density and the solar wind speed at all latitudes, *J. Geophys. Res.*, **86**, 8869.
- Smirnova, T.V., Chashei, I.V., Shishov, V. I.: 2009, Radio sounding of the circumsolar plasma using polarized pulsar pulses, *Astron. Rep.*, **53**, 252 (doi:10.1134/S106377290903007X).
- Tiburzi, C., Verbiest, J.P., Shaifullah, G.M., Janssen, G.H., Anderson, J.M., Horneffer, A., Künsemöller, Osłowski, Donner, J.Y., Kramer, M., Kumari, A., Porayko, N.K., Zucca, P., Ciardi, B., Dettmar, R.-J., Griefmeier, J.M., Hoefft, M., Serylak, M.: 2019, On the usefulness of existing solar wind models for pulsar time corrections, *Mon. Not. Roy. Astron. Soc.*, **487**, 397 (doi:10.1093/mnras/stz1278).
- Tokumaru, M.: 2013, Three-dimensional exploration of the solar wind using observations of interplanetary scintillation, *Proc. Jpn. Acad. Ser. B.*, **89**, 67 (doi:10.2183/pjab.89.67).
- Tokumaru, M., Kojima, M., Fujiki, K., Hayashi, K.: 2009, Non-dipolar solar wind structure observed in the cycle 23/24 minimum, *Geophys. Res. Lett.*, **36**, L09101 (doi:10.1029/2009GL037461).
- Tokumaru, M., Kojima, M., Fujiki, K.: 2010, Solar cycle evolution of the solar wind speed distribution from 1985 to 2008, *J. Geophys. Res.*, **115**, A04102 (doi:10.1029/2009JA014628).
- Tokumaru, M., Kojima, M., Fujiki, K., Maruyama, K., Ito, H., and Iju, T.: 2011, A newly developed UHF radiotelescope for interplanetary scintillation observations: Solar Wind Imaging Facility, *Radio Sci.*, **46**, RS0F02 (doi:10.1029/2011RS004694).
- Tokumaru, M., Kojima, M., Fujiki, K.: 2012, Long-term evolution in the global distribution of solar wind speed and density fluctuations during 1997–2009, *Journal Geophys. Res.*, **117**, A06108 (doi:10.1029/2011JA017379).
- Tokumaru, M., Fujiki, K., Iju, T.: 2015, North-south asymmetry in global distribution of the solar wind speed during 1985–2013, *J. Geophys. Res.*, **120**, 3283 (DOI:10.1002/2014JA020765).
- Tokumaru, M., Shimoyama, T., Fujiki, K., Hakamada, K.: 2018, Rarefaction of the very-slow (<350 km/s) solar wind in Cycle 24 compared with Cycle 23, *J. Geophys. Res.*, **123**, 2520 (doi:10.1002/2017ja025014).
- Weisberg, J.M., Payne, R.R., Counselman, C.C.: 1976, Further changes in the distribution of density and radio scattering in the solar corona in 1973, *Astrophys. J.*, **209**, 252 (doi:10.1086/154715).

**Table 1.** Characteristics of the Crab pulsar

Right ascension (J2000)	05 h 34 m 31.97 s
Declination (J2000)	+22° 00' 52.1"
Period	33.4 ms
Logarithm of the period derivative	-12.4
Distance	2 kpc
Typical DM value	56.79 pc cm <sup>-3</sup>

**Table 2.** Observation parameters

---

Time span (UT)	19/09/2017 – 15/07/2018
Observation cadence	1 /day
Duration of observations	360 s
Frequency	327 $\pm$ 10 MHz
Sampling rate	256 Msps
Bit depth	8

---

**Table 3.** Number of GPs with  $S/N > 15$ ,  $N$ , and DMs. The date is shown as year, month, day altogether.

Date (UT)	MJD (UT)	$N$	DM ( $\text{pc cm}^{-3}$ )
20170919	58015.85	29	$56.760 \pm 0.005$
20171014	58040.78	38	$56.763 \pm 0.003$
20171114	58071.70	26	$56.761 \pm 0.003$
20171219	58106.60	46	$56.758 \pm 0.003$
20180115	58133.53	38	$56.756 \pm 0.001$
20180215	58164.45	24	$56.756 \pm 0.002$
20180315	58192.37	21	$56.760 \pm 0.002$
20180415	58223.28	13	$56.757 \pm 0.003$
20180515	58253.20	7	$56.764 \pm 0.013$
20180601	58270.16	25	$56.748 \pm 0.013$
20180614	58283.12	14	$56.760 \pm 0.007$
20180615	58284.12	5	$56.766 \pm 0.014$
20180616	58285.12	6	$56.769 \pm 0.009$
20180617	58286.11	9	$56.768 \pm 0.007$
20180618	58287.11	9	$56.750 \pm 0.006$
20180619	58288.11	8	$56.773 \pm 0.005$
20180701	58300.07	29	$56.762 \pm 0.008$
20180715	58314.04	14	$56.758 \pm 0.014$

**Table 4.** Summary of coronal density models deduced from pulsar DM measurements

Year	Solar Activity	$N_0$ [ $10^3 \text{ cm}^{-3}$ ]	$\alpha$	Reference
1969, 1970	SC20 maximum	$7.0 \pm 0.6$	$2.9 \pm 0.2$	Counselman and Rankin (1972)
1971	SC20 maximum	$5.0 \pm 0.6$	$1.4 \pm 0.3$	Counselman and Rankin (1973)
1973	SC20 declining	$5.2 \pm 0.2$	$\simeq 2.0$	Weisberg, Payne, and Counselman (1976)
1990	SC22 maximum	$6.8 \pm 1.8$	$1.5 \pm 0.8$	Cognard <i>et al.</i> (1996)
1991	SC22 maximum	$9.7 \pm 1.3$	$2.7 \pm 1.0$	Cognard <i>et al.</i> (1996)
1992	SC22 declining	$7.3 \pm 1.0$	$2.6 \pm 0.7$	Cognard <i>et al.</i> (1996)
1993	SC22 declining	$5.2 \pm 0.9$	$1.4 \pm 0.4$	Cognard <i>et al.</i> (1996)
2007	SC23/24 minimum	$3.0 \pm 1.8$	$2.6 \pm 0.2$	Smirnova, Chashei, and Shishov (2009)
2018	SC24/25 minimum	$7.8 \pm 7.9$	$1.7 \pm 1.3$	This study



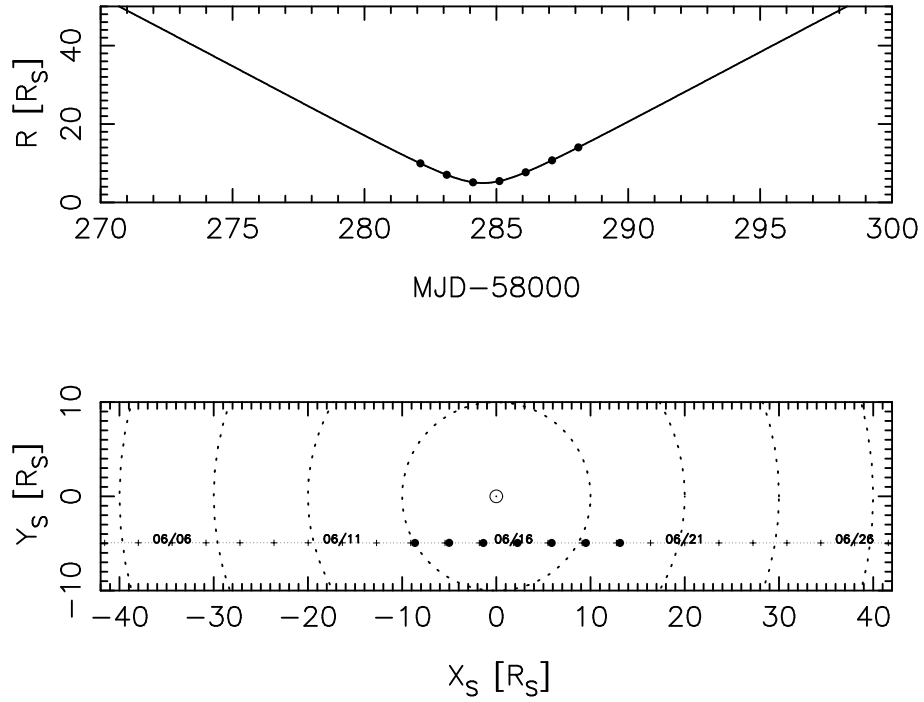


**Figure 1.** Time variation of (upper) solar offset distances and (lower) plane-of-sky locations of LOS for the Crab pulsar in June 2018. Solid circles correspond to the times when Crab pulsar observations were made at Toyokawa. Dotted circles correspond to constant solar offset distances drawn every  $10 R_S$ .

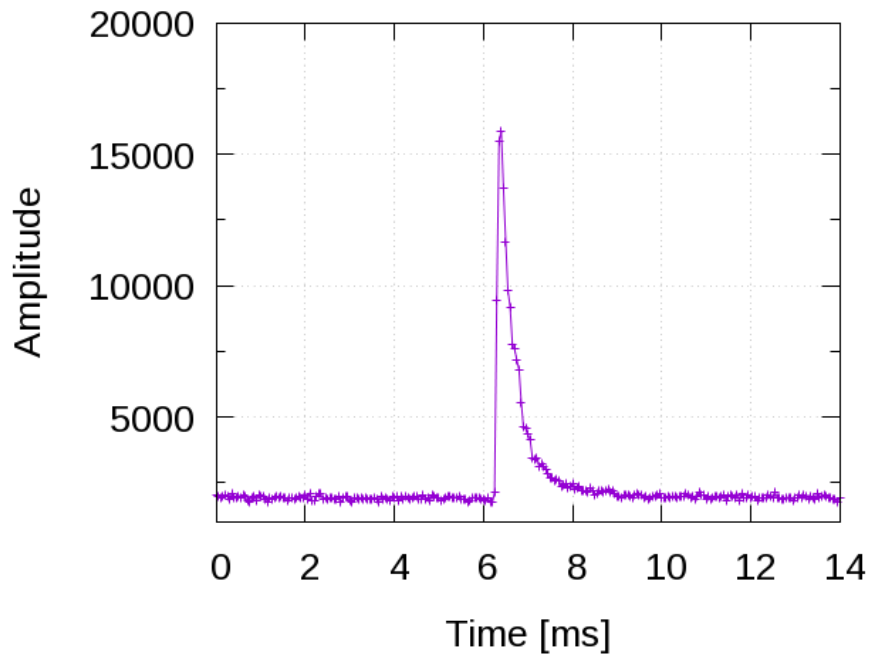


**Figure 2.** The giant pulse detected from Crab pulsar observations on 20 September 2018 at Toyokawa. The amplitude is given in arbitrary units.

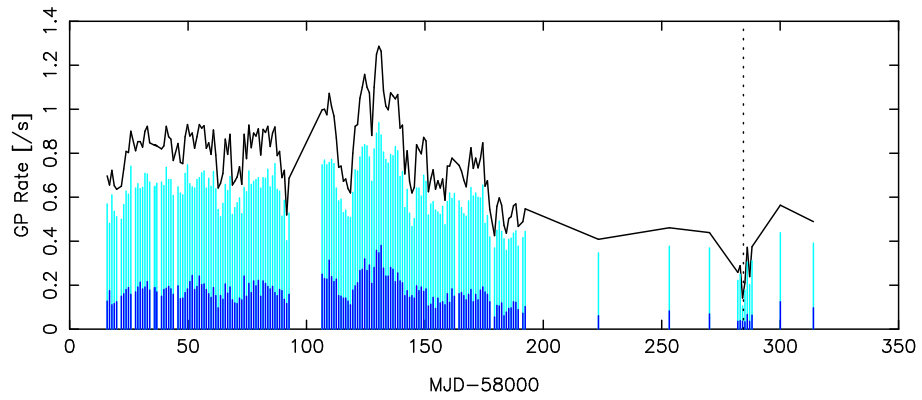


**Figure 3.** Time variation of GP rates with  $S/N > 5$ . Cyan and blue vertical bars denote MP and IP GPs, respectively. The solid black line indicates total (MP+IP) GP rates. The vertical dotted line indicates the time of the closest approach of the Crab pulsar's LOS to the Sun.

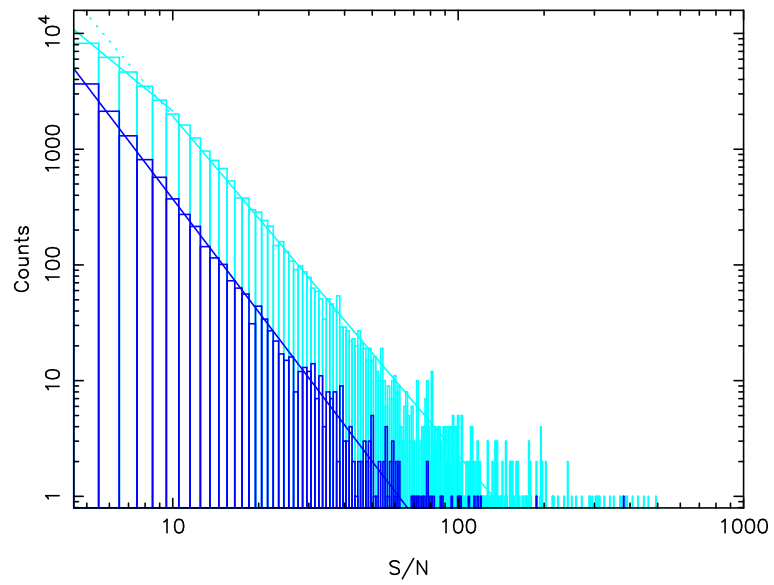


**Figure 4.** Histogram of S/N for MP (cyan) and IP (blue) GPs. Oblique solid lines represent the best-fit power-law functions.

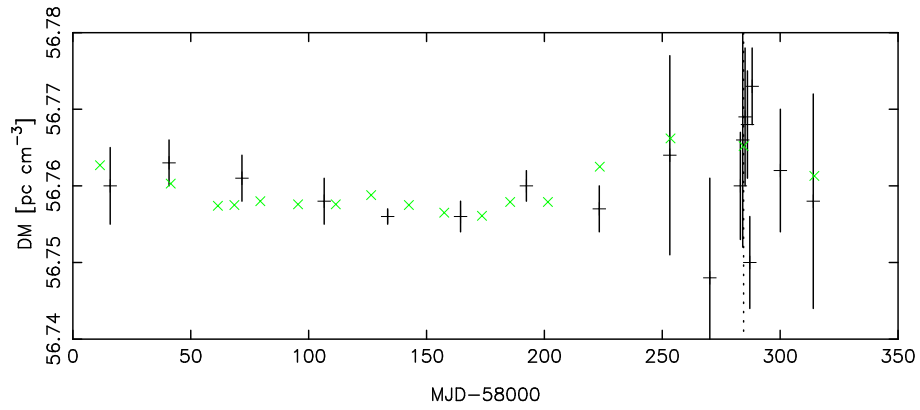


**Figure 5.** Time variation of DMs determined from Crab pulsar observations at Toyokawa (black crosses) and Jodrell Bank (green x-symbols). Vertical bars on the Toyokawa DM data indicate rms deviations.

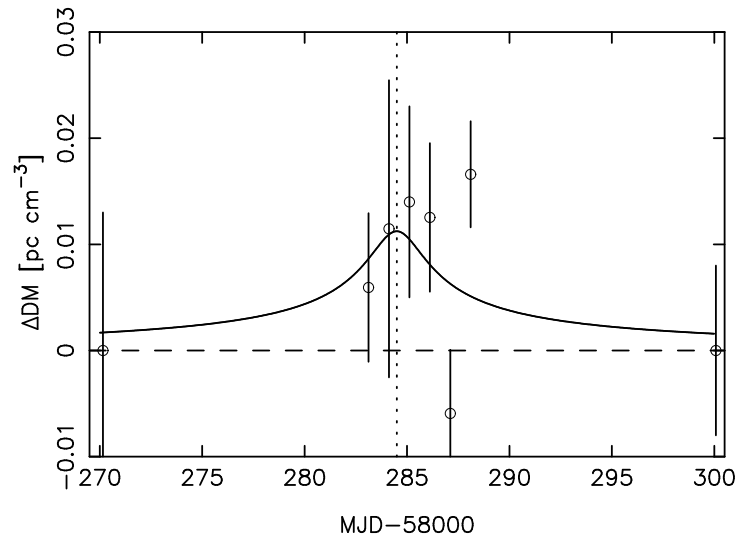


**Figure 6.** Time variation of  $\Delta\text{DM}$  for the period around the closest approach of the Crab pulsar's LOS to the Sun (vertical dotted line).

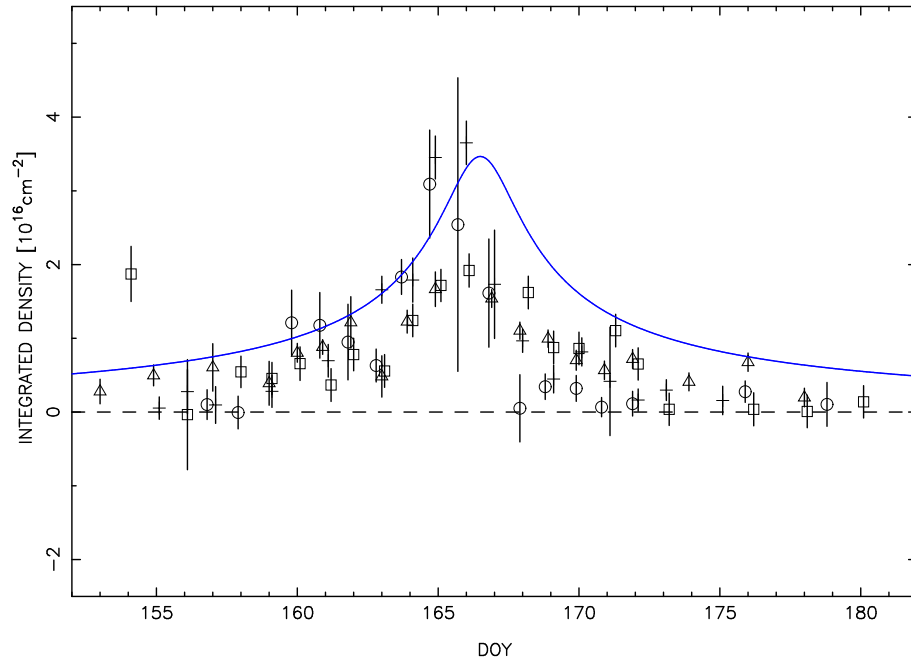


**Figure 7.** Comparison of coronal density data derived from Crab pulsar observations. The solid line indicates the density model determined from the present study. The cross, circle, square, and triangle denote Crab pulsar observations made at Arecibo in 1996, 1970, 1971, and 1973, respectively (adopted from Counselman and Rainkn, 1972, 1973, and 1976).

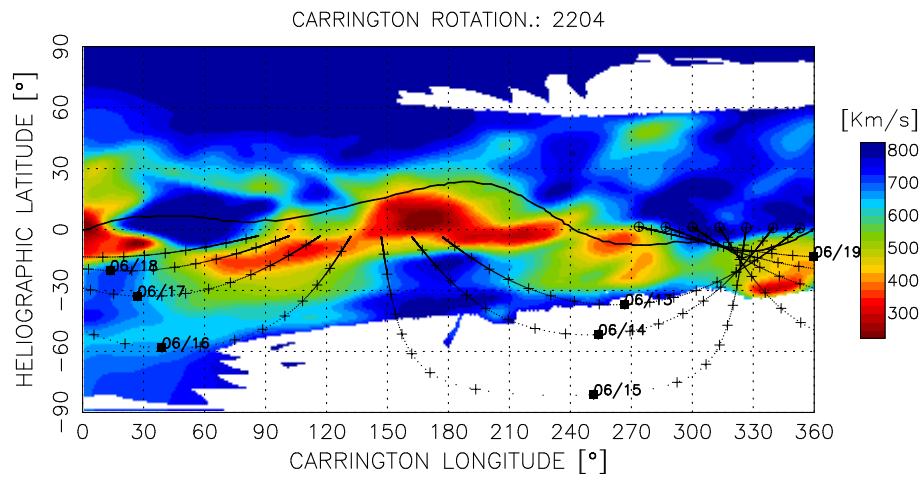


**Figure 8.** Synoptic source surface map of the solar wind speed derived from ISEE IPS observations for CR 2204. The dotted lines indicate trajectories of LOS projected on the source surface for the period between 13 and 19 June 2018. The solid square on each LOS indicates the location of the P-point. The solid line indicates the magnetic neutral line derived from magnetograph observations at the Wilcox Solar Observatory (WSO).



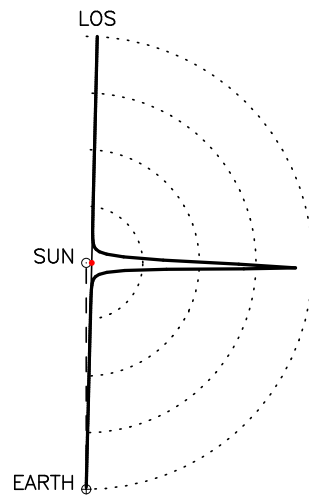


**Figure 9.** Schematic of the solar wind density variation (thick line) along the LOS for the P-point distance of  $5 R_S$ . The density is assumed to be distributed as  $r^{-2}$ . The location of the P-point is indicated by a red circle.

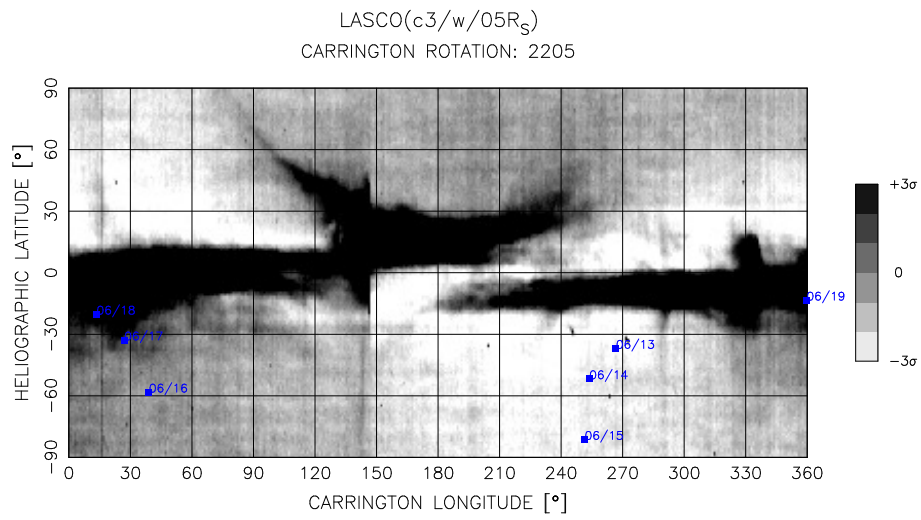


**Figure 10.** Synoptic Carrington map of the solar corona at 5  $R_S$  derived from LASCO C3 (west limb) observations for CR 2205. The solid blue squares indicate the projected locations of the P-point on the LOS of the Crab pulsar during 13 and 19 June 2018.

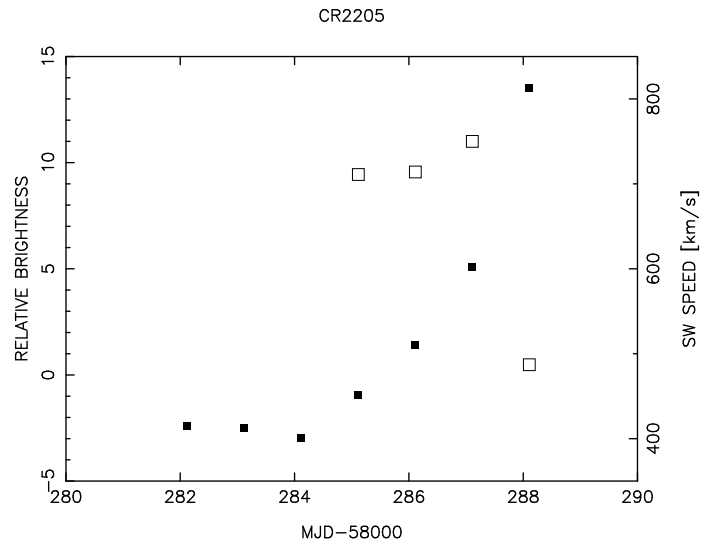


**Figure 11.** Time variation of the solar wind speed (open squares) and whitelight brightness (solid squares) at the P-points of LOS for the Crab pulsar.